



Review

Nanoplasmonics in Catalysis for Energy Technologies: The Concept of Plasmon-Assisted Molecular Catalysis (PAMC)

Constantinos Moularas ¹, Aikaterini Gemenetzi ², Yiannis Deligiannakis ^{1,*} and Maria Louloudi ^{2,*}¹ Department of Physics, University of Ioannina, 45100 Ioannina, Greece; km1700@eohsi.rutgers.edu² Department of Chemistry, University of Ioannina, 45100 Ioannina, Greece; yemenetzi.k@gmail.com

* Correspondence: ideligia@uoi.gr (Y.D.); mlouloud@uoi.gr (M.L.)

Abstract: The utilization of plasmonic nanomaterials in catalytic technologies is an emerging research field with foreseeable applications in energy-catalytic technologies. On this front, the coupling of plasmonic nanomaterials with molecular catalysts is a newly approached, thus far unexploited field, that we discuss herein. In the present mini review, we contrast the case where the plasmonic particle itself is the catalytic center against the case where the plasmonic particle acts as a co-catalyst for an operational catalytic system. In the first part, we present an outline of the key phenomena in nanoplasmonics, and their potential implications in catalytic processes. The concepts of hot electrons, hot holes, and the dynamics of their generation and transfer are reviewed, as are the contribution of near-field and photothermal effects to catalytic processes. All these plasmonic-phenomena are then discussed in conjunction with representative catalytic systems from the literature.

Keywords: nanoplasmonics; molecular catalysts; nanohybrids; PAMC; LSPR; hot electrons; photocatalysis; hydrogen; oxidation catalysis



Citation: Moularas, C.; Gemenetzi, A.; Deligiannakis, Y.; Louloudi, M. Nanoplasmonics in Catalysis for Energy Technologies: The Concept of Plasmon-Assisted Molecular Catalysis (PAMC). *Nanoenergy Adv.* **2024**, *4*, 25–44. <https://doi.org/10.3390/nanoenergyadv4010002>

Academic Editors: Juan M. Coronado and Ya Yang

Received: 22 October 2023

Revised: 25 December 2023

Accepted: 26 December 2023

Published: 30 December 2023



Copyright: © 2023 by the authors. Licensee MDPI, Basel, Switzerland. This article is an open access article distributed under the terms and conditions of the Creative Commons Attribution (CC BY) license (<https://creativecommons.org/licenses/by/4.0/>).

1. Introduction

The global energy crisis mandates the adoption of clean energy technologies, based on renewable sources such as sunlight. To this end, two key issues can be considered among forward-looking solutions: [i] one is exploitation of the full spectrum of solar photons, since the highest efficiency of sunlight energy conversion into chemical activity has so far almost exclusively been confined to the utilization of UV-absorbing TiO₂-based nanomaterials [1]. In years, there mounting evidence has emerged that plasmonic nanomaterials can provide a decisive boost to photo-driven reactions [2]. In brief, the underlying physics of plasmonic nanostructures and their action as “antennae” can be outlined as follows: the incoming light can be concentrated in nanoscale volumes, thus giving rise to collective oscillations of electrons, a phenomenon known as localized surface plasmon resonance (LSPR) [3]. Consequently, locally intense electric fields (hot spots) at the particle–particle interface, form an ideal active site for chemical processes to occur [4,5]. The plasmonic effect also generates hot carriers [6], namely highly energetic photoinduced e[−]–h⁺ pairs. Moreover, the stored quanta of energy in the oscillating charge density during LSPR can be dissipated via several mechanisms and utilized in different ways [7], such as the photothermal effect, i.e., heat generation from the photo-excited plasmonic nanoparticles (PNPs) [8] (Figure 1). Thus, the plasmonic phenomenon manifests in different ways, and each of them can be utilized in different types of catalytic processes [9]. These properties of plasmonic nanoparticles render them highly attractive for various applications, including sensing, imaging, and enhancing light–matter interactions.

In recent years, numerous review articles have been published focusing on catalytic applications where the plasmonic materials themselves act as catalysts for a wide range of catalytic reactions [10–12]. In particular, the local temperature increase around PNPs has led to, for example, applications in nanomedicine, for tumor targeting [13,14], or in catalysis

for the thermal acceleration of reactions [15]. The LSPR-induced local electric field in close proximity to the PNPs is another intriguing property that has been utilized for surface-enhanced Raman scattering (SERS) spectroscopy [16], sensor-related applications [17,18], and catalysis [19,20]. Finally, in the context of catalysis, the generation of hot carriers by plasmonic nanostructures is the most widely exploited mechanism [21]. Gold (Au^0), silver (Ag^0), copper (Cu^0), and aluminum (Al^0) are the most common metals possessing measurable LSPR properties, giving birth to the field of plasmonic catalysis [22]. The coupling of plasmonic materials with catalytic metals (e.g., Pt, Pd, etc.) can promote the transfer of electrons from a PNP to the catalytic metal, for example, via LSPR-induced local electric fields in the PNP's vicinity [23].

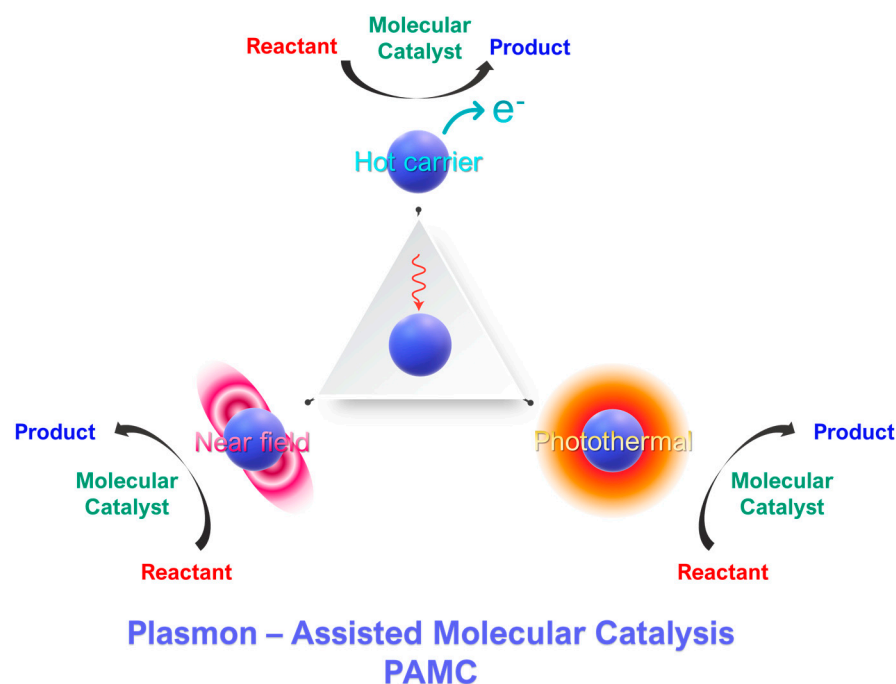


Figure 1. Concept of plasmon-assisted molecular catalysis (PAMC). Molecular catalysts perform a specific catalytic reaction. Photoexcited plasmonic nanoparticles can intervene in the catalytic process via three mechanisms: [i] generation of hot carriers and [ii] the photothermal effect of [iii] near-field effects.

From a forward-looking perspective, the combination of plasmonic nanoparticles with molecular catalysts is an emerging research field with significant potential for various catalytic applications. Herein, our aim is to present the first review on the field plasmon-assisted molecular catalysis (PAMC)—see the concept outline in Figure 1. Thus, for the sake of clarity, we conceptualize PAMC as those cases where a molecular catalyst is the key catalytic entity and the plasmonic particles exert an auxiliary effect on the catalytic process. As we discuss, this effect does not always boost the catalysis, and it can result in a reversible pause of the catalytic process.

Although the literature concerning this subject has, thus far, remained highly limited, it is possible to realize the potential of PAMC systems by studying the interaction between plasmonic nanoparticles and simpler moieties. For instance, there is extensive research on the interaction and catalytic behavior of plasmonic nanostructures with small molecules [24]. Considering all of the above, it is evident that, depending on the molecular moiety and its catalytic function, a different feature of plasmonic structures can be employed, from simply acting as a thermal source to inducing redox phenomena in more complex systems. For completeness, we can cite numerous interdisciplinary reviews focusing on the implementation of plasmonic materials as catalysts themselves in energy-related catalysis such as solar cells [25], CO_2 reduction [26], environmental remediation [27], H_2O

splitting [28], photocatalysis [22,29,30], as well as plasmonic catalysts [31]. In this mini review, we focus on the PAMC where the catalysis performed by the molecular catalyst is quantified by indices classically used in molecular catalysis such as turn over numbers (TONs) and turn over frequencies (TOFs), etc.

2. Fundamentals of the Plasmonic Phenomenon

To trigger plasmon-enhanced chemical activity, the plasmonic mechanisms derived by illuminating metallic nanoparticles need to have been thoroughly understood. Considering the multiple degrees of freedom in these systems, properly distinguishing the relative contributions of each plasmonic mechanism to a given reaction can be quite challenging. The scope of the present mini review is not the detailed disentanglement of every plasmonic phenomenon, shown in Figure 2, but to provide a comprehensive classification in order to facilitate a better understanding and interpretation of the underlying mechanisms. In this context, we can classify the plasmonic phenomena into three families: [i] those evidenced from “outside the particle”, i.e., these are mainly phenomena involving light scattering [32]; [ii] those evidenced from “inside the particle”, which refers to the hot electrons and holes generated by the decay of photoexcited plasmon modes inside the particle [33]; and [iii] those evidenced at the particle–particle interface, i.e., also involving the presence of hot spots [34]. On that point, the required energy that activates these plasmonic reaction channels originates from the oscillating motion of a metal’s free electrons, storing energy in quanta also known as plasmons. In LSPR, the restricted motion of electrons in the particle–environment nano-interface gives birth to new energy transfer pathways, which are, herein, summarized according to the occurrence of each phenomenon, i.e., outside, inside, and the interface of the plasmonic nanostructure, as depicted in Figure 2.

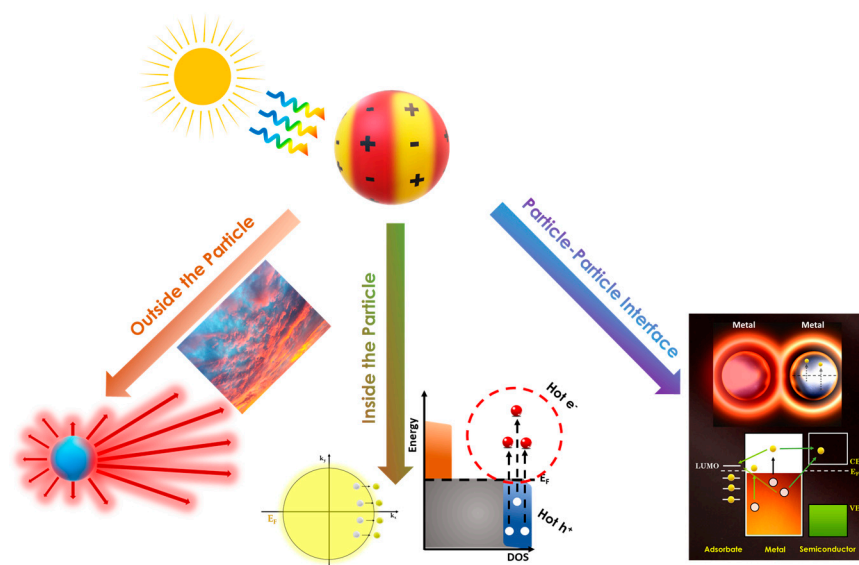


Figure 2. A schematic depicting the plasmon-driven mechanisms regarding the scale at which they occur. The LSPR-induced energy dampens through radiative phenomena outside the particle (light scattering) and non-radiative phenomena inside the particle (hot-carrier generation) and at the particle–particle interface (thermal effects, electric fields, and charge transfer to near acceptors).

Starting from outside the particle, the response of the electron density to an external electromagnetic wave, i.e., light, and the subsequent light-scattering phenomena are classically described by the Drude model [35] and Mie theory [36], respectively, for the case of a single nanosphere. Although this is the least interesting plasmon event in catalysis, Mie theory established control over the optical properties of the plasmonic nanostructures by adjusting the particle size, shape, and dielectric properties of the metal and surrounding medium [37–40]. Furthermore, the Mie absorption cross-section is the starting point that describes how the plasmonic metal’s electrons gain energy from this light-matter

interaction, i.e., the energy that eventually will be transferred to a catalytic active site. In this regard, it is clear that plasmonic effects can be distinguished to radiative and non-radiative processes [41], see Figure 2. In a radiative process, LSPR relaxes and re-radiates light into the far field, thus the metal nanostructures can act as a secondary light source (“antenna”) that concentrates light on the particle surface and enhances local electric fields in its proximity. In the case of the non-radiative process, plasmon dephasing causes photon absorption that deposits electronic energy in the electron cloud inside the particle, which in turn results in highly energetic electrons with energy above the Fermi level—so-called “hot” electrons [6,33]. These routes of plasmon energy dissipation will be described in more detail in the following section.

Photoinduced plasmonic hot carriers are electrons in a metallic particle follow the Fermi–Dirac distribution. Figure 3 exemplifies the case of Ag^0 nanoplasmonics, which contain electrons in the sp-band as well as in the d-band. The photoexcitation process in plasmonics is more complex than in typical semiconductors [40]. The key idea is that the decay of the plasmons creates the electronic excitations/pathways which, in a broad context, can be involved in catalytic processes. Thus, understanding plasmon creation and decay is of crucial importance for the connection between plasmonic phenomena and catalysis, see Figure 4. Hereafter, we provide a short comprehensive overview of the fundamentals.

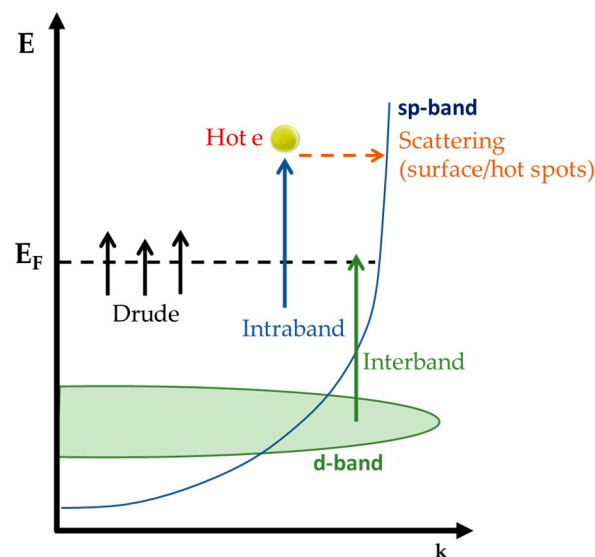


Figure 3. The allowed electro-transitions in the case of photoexcited metallic Ag^0 nanoparticles. The arrows describe the main plasmon energy damping channels, occurring after plasmon decay.

When PNPs are illuminated by discrete photons with energy $\hbar\omega$, photon absorption in this light–matter interaction is impossible because such transitions require additional momentum through inelastic scattering (e.g., with a lattice defect or a lattice phonon) or occur in a confined system with boundaries (backscattering events), as shown in Figure 3 [42,43]. In addition to the dynamics of charge carriers in a metal, the effects of quantum confinement in small particles should be considered.

The first immediate consequence of this transition is that the current created by the electromagnetic field will accumulate electric charge at the surface of the particle. In the classical picture, these charges would accumulate solely at the surface of the particle, but in realistic systems, the charges at the interface extend into a non-zero volume inside the metal, screened and interacting with other mobile charges. Therefore, by decreasing the particle size, the quantum effects at the surfaces become more relevant over plasmon dynamics [44]. Specifically, they contribute to plasmon dephasing, with the coherent collective oscillation

of the carriers inside the metal decaying into incoherent electronic excitations [32], see Figure 4. This is parametrized by Equation (1)

$$\gamma_{surf} = A \frac{u_F}{R} \tag{1}$$

where γ_{surf} is the surface-assisted damping factor of the plasmons, A is an empirical constant ~ 1 , u_F is the metal's Fermi velocity, and R is the particle radius [32]. More generally, the surface-induced damping arises from electron collisions with the particle's boundaries [45,46]. The boundary discretizes the electronic states inside the metal [45,46]. Then, the surface allows a breaking of the momentum conservation by discretizing the electronic states in the particle, a process known as surface-assisted plasmon decay or Landau damping [45,46]. It is this anelastic scattering that allows excitation of hot electrons with energies E_{HE} higher than the Fermi level, ranging in the interval [47], see also Figure 4,

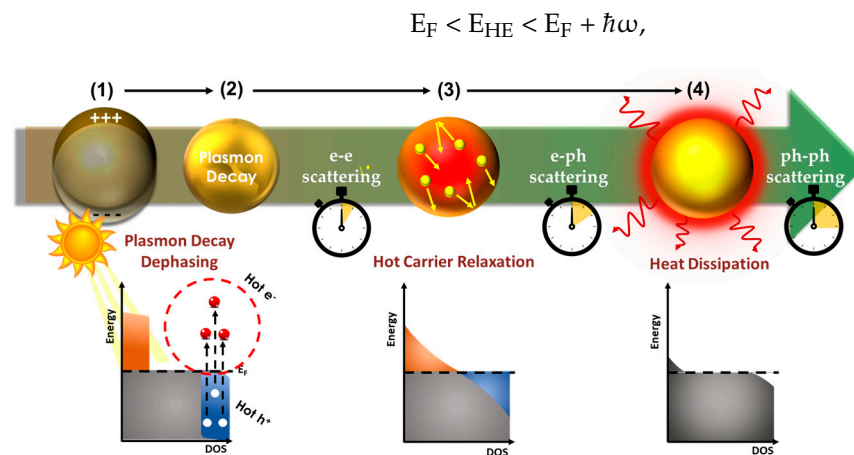


Figure 4. Hot-carrier relaxation events (from left to right): (1): absorption of light photons excites plasmons, which decay and stimulate the creation of [hot electron]–[hot hole] pairs. Some of the hot electrons attain energy above the Fermi level. These can participate in catalytic processes. Subsequently, (2) the hot carriers relax via electron–electron scattering, and then they equalize their temperature with the lattice vibrations via electron–phonon scattering, (3) all this in a few ps. Finally, (4) the relaxation of the hot lattice is achieved via phonon–phonon interactions, where the stored energy in the vibrational modes is dissipated from the nanoparticle to the surrounding medium as heat, i.e., leading to a rise in temperature. This can contribute thermal input to catalytic processes.

Thus, the generation of hot carriers can be controlled by modifying the size and shape of the metallic particle [48–50]. Another factor that correlates to surface confinement, and hence the stimulation of hot carriers, is the presence of the intense electric fields in the vicinity of the particle's boundary (hotspots) [34]. When this local field distribution is concentrated in sharp features of the nanostructure or in nanogaps, in the case of coupled PNPs, the plasmonic field significantly amplifies the population of nonthermal carriers [51–53].

More generally, the creation of hot carriers in metallic nanoparticles depends on the lossy nature of the LSPR process, i.e., the way the plasmons decay. Hence, overall plasmon decay involves all non-radiative decay mechanisms expressed by the plasmon lifetime as [54]

$$\gamma_{plasmon} = \gamma_{Drude} + \gamma_{interband} + \gamma_{surf} + \gamma_{HotSpots} + \gamma_{rad} \tag{2}$$

where γ_{Drude} is the term for the electron–electron and electron–phonon interaction following the classical electrodynamic picture of coherent charge oscillation. $\gamma_{interband}$ is the term for the direct optical transitions (typically from the d to sp band in the case of Ag and Au), which is not included in the classical model. The previously described surface and hotspot effects are included in γ_{surf} and $\gamma_{HotSpots}$, respectively. In contrast to the other terms, γ_{rad} is the term for radiative losses, where light is re-emitted in the far-field.

When the light-induced plasmon energy is not shared with other systems with any of the aforementioned pathways, the following relaxation events dampen the plasmon resonance until the energy is dissipated as heat (shown in Figure 4): [55,56].

- Step 1: Electronic thermalization, hot electron generation

The decay of light-induced plasmons stimulates the creation of electron–hole pairs above the Fermi level. These are called “hot electrons” and “hot holes”, since this can be a highly energetic process with energies in the range of several eV. To put this in the context of catalytic processes, we should consider that typical covalent-bond energy is in the range ~100–400 kJ/mole that, by the conversion factor 1 eV = 96 kJ/mole, is ~1–4 eV. The rest of the electrons decay via a plasma decay-type process, i.e., plasma = the hot electron cloud inside the particle, bringing the electron plasma to an equilibrium state at a high temperature, within fs [57]. We underline that this is an internal process, i.e., occurring inside the plasmonic particle, thus it is rather unlikely to contribute directly in a catalytic process.

- Steps 2,3: Hot carrier relaxation

The following stage involves the conversion of electronic energy to vibrational energy via electron–phonon interactions [58] where the plasma relaxes and equalizes its temperature with the particle lattice vibrations. As a result, the equilibrium inside the particle has been restored, as the electron gas temperature matches the crystal lattice temperature, and internal thermal homogeneity has been achieved [59]. The particle size influences the timescale of electron–phonon interactions as demonstrated by Hartland et al. [55] and Link and El-Sayed [59].

- Step-4: Lattice relaxation, heat generation

Finally, the relaxation of the hot lattice is achieved via phonon–phonon interactions, where stored energy in the vibrational modes is dissipated from the nanoparticle to the surrounding medium. This is the step where heat is provided to the surrounding medium, leading to a temperature rise in the immediate vicinity of the PNP, known as a “thermoplasmonic” process [60]. The thermoplasmonic process may be very important in catalysis, since it may provide a direct heat source to the catalysis system.

Govorov and co-workers and Manjavacas et al. highlighted the influence of particle size on hot carrier generation rate and on energy distribution [48,54]. Specifically, Figure 5 demonstrates that despite being larger, Ag particles excite more electrons, since they are low-energy, Drude-like carriers. By decreasing particle size, surface effects dominate and plasmons decay into high-energy electrons, although the population of hot carriers remains low compared to Drude carriers [48,54]. In the case of 2 nm particles, the overall carrier population is lower than that of the larger particles but the relative concentration of hot and Drude carriers is almost equal.

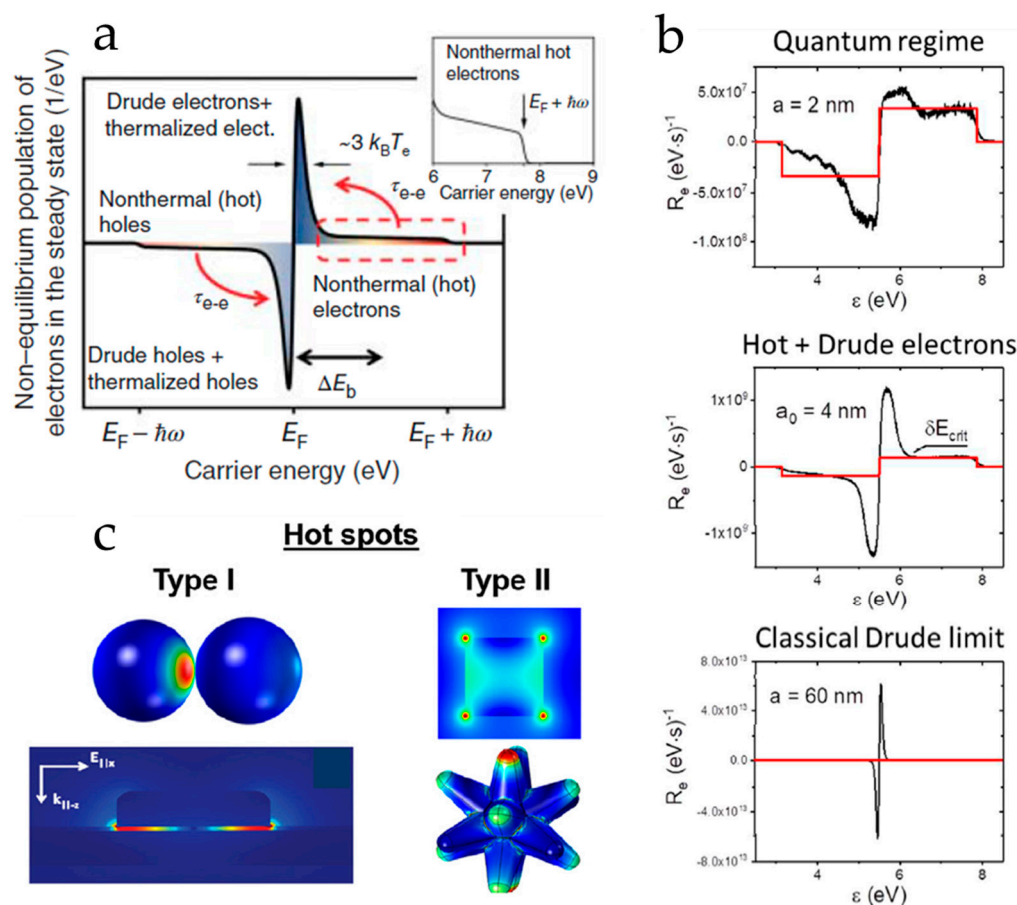


Figure 5. The hot-carrier population as a function of (a) energy distribution and (b) the particle size. (c) Hot spots formed in the nanogaps (Type I) or sharp features of nanostructures (Type II). ((a) and (c): Adapted with permission from Ref. [61], 2019, ACS; (b): Adapted with permission from Ref. [54], 2017, ACS.).

Hotspots: In contrast to the non-radiative process, in a radiative process [41] (see Figure 2), plasmon excitation relaxes via the re-radiation of light into the far-field, thus metal nanostructures can act as secondary light sources (“antennas”) that concentrate light on the particle surface and enhance local electromagnetic (EM) fields in their close proximity. In turn, hot carrier generation depends on the electric fields on the particle surface [54]. Specifically, hotspots formed in coupled PNPs and/or sharp geometrical features in the PNP shape increase the number of hot electrons drastically [54,62–64]. These local electric fields can enhance catalytic processes too. Here we must understand that this can happen only in the proximity of the hotspot, which means the catalytic process should occur on the particle–solution interface rather in the bulk. We have explained, this holds true for the case of plasmon-enhanced hydrogen atom transfer in hybrid nano-antioxidants such as SiO₂@Ag-[Gallic Acid] [65].

3. How Plasmonic Catalysis Works

So far, plasmonic nanostructures have been incorporated into catalytic systems in many ways. Therefore, “plasmonic catalysis” has become an umbrella term for catalytic systems that utilize a plasmonic component. This can happen using: [i] stand-alone plasmonic catalysts or [ii] plasmonic structures in conjunction with a heterogeneous (nano)catalyst or molecular catalyst. In the first case, the plasmonic structure has a dual role, both absorbing light and catalyzing the desired reaction. Plasmonic nanostructures have been used in a variety of different catalytic systems, acting as the catalyst themselves [66–71] or utilizing high light intensities. Up to now, in most cases, plasmonics have been used in electrochemi-

cal and/or photochemical reactions [72,73] or gas-phase reactions at high temperatures [74]. In fact, the lack of selectivity is a challenge for plasmon-assisted reactions [23,66,75–79].

In the second case, there is a more complex system with a plasmonic component and a second structure that acts as the catalyst. When the second structure is a heterogeneous catalyst, there can be various heterostructures forming the final catalytic material, depending on its spatial structure. Thus, there can be A@B structures (A: catalyst, B: plasmonic metal), A-B core-shell structures, or AB alloy structures (Figure 6). In the majority of these combination systems, there is a conjunction of plasmonic structures with semiconductors [80–83]. In the case of plasmon-assisted molecular catalysis (PAMC), a plasmonic nanostructure can be used in tandem with a molecular catalytic moiety [84–86], giving birth to a new and promising concept in the field of catalysis.

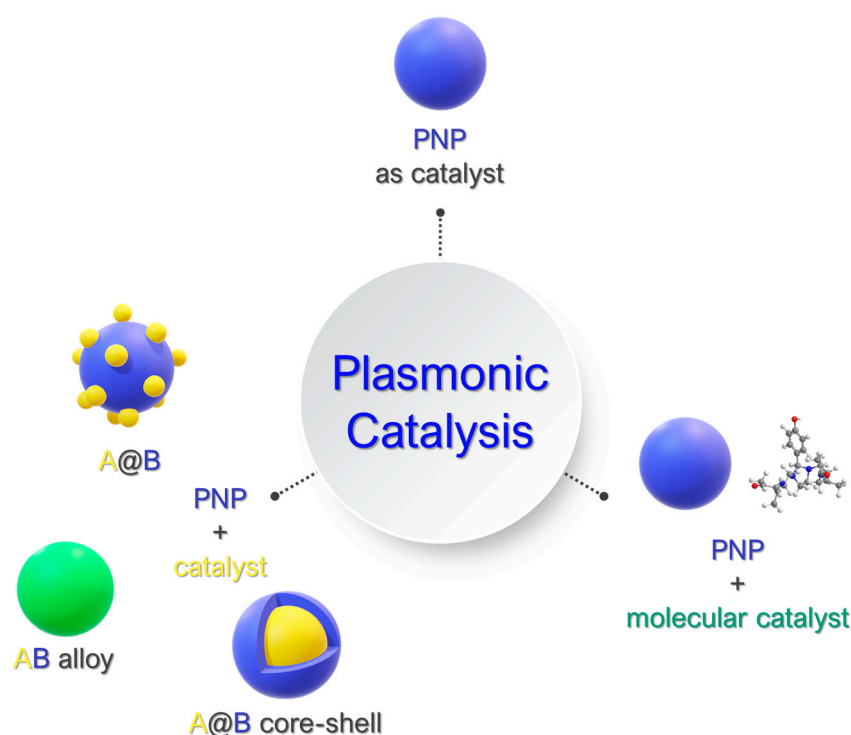


Figure 6. Schematic representation of the different catalyst designs for PNP-activated hydrogenation catalysis.

In this context, it has been shown that plasmonic Ag and Au can act as the light controller and electron supplier to adsorbate molecules accelerating chemical transformations [87,88], despite the poor catalytic activity of stand-alone Ag or Au. In this case, [89,90], the surface-assisted plasmon dephasing results in the stimulation and transfer of high-energy nonthermal electrons, that induce the activation of the adsorbed species via vibrational excitation. When the kinetic energy is sufficient, these hot electrons are injected into the lowest unoccupied orbital of the adsorbate (LUMO). It is important to highlight that low-energy Drude electrons cannot overcome the interfacial barrier, thus they are transferred to the adsorbate. The constantly expanding literature has showcased the enhanced chemical activity in adsorbed species, induced by the excitation of hot holes [91–106] and hot electrons [90,96–109], with some pertinent case-studies listed in Table 1.

Table 1. Key cases on the mechanistic insight of plasmonic catalysis.

Reaction	Material	Mechanism	Reference
H ₂ dissociation	Au, Au/SiO ₂ , Al	Weakening the H–H bond due to accumulated hot electrons	Halas [110–112]
O ₂ dissociation	Ag	Depositing energy in the O–O bond due to hot electron back-and-forth transfer	Christopher et al. [74]
MB decomposition/desorption	Ag	Direct electron transfer involving hybridized Ag-MB electronic states	Boerigter et al. [113]
CO ₂ Reduction	Au/Al ₂ O ₃ /TiO ₂	Controlled synergy of hot electrons/near-field enhancement by tuning the Al ₂ O ₃ shell thickness	Zhao et al. [89]
C-F dehydrofluorination	Al-Pd	Enhanced Pd optical absorption caused by the near-fields of the plasmonic Al antenna	Robatjazi et al. [90]
Formic Acid Dehydrogenation	Au-Pd	Plasmon-assisted reduction of adsorbed H atoms and the C–H cleavage bond of the FA [−]	Herran et al. [114]
Fe ³⁺ Reduction	Au	e/h formation due to the synergistic interband (d-sp) and intraband (hot carriers) transitions	Kim et al. [115]
Alkene Epoxidation	Ag@SiO ₂	Hot-carrier-assisted, on-demand pause of oxidation by inhibiting the LMn ^{IV} = O intermediate	Gemenetzi et al. [84]
Cr ⁶⁺ Reduction	Ag@SiO ₂	Light-driven decrease of the activation barrier and hotspot-assisted generation of hot electrons	Moularas et al. [116]
Formic Acid Dehydrogenation	Ag@SiO ₂	Hot electron-induced lowering of the solution potential	Gemenetzi et al. [85]

Among them, the pioneering work of Halas' group demonstrated the plasmon-mediated dissociation of adsorbed H₂ species [110]. Using Au nanoparticles under visible light, they have shown that the kinetic energy of the excited nonthermal carriers overcomes the large activation energies and drives the catalytic process at room temperature. Initially, the nonthermal hot electrons are injected into antibonding orbitals of the H₂ molecule; however, due to their short lifetime, they are transferred back to the Au. The H–H bond stretching induced by the accumulated vibrational energy leads to H₂ dissociation. Furthermore, the same group provided evidence that the dissociation occurs on the Au surface by changing the substrate (TiO₂, SiO₂) [111], normalizing any charge transfer between the Au and the substrate [117]. Also, the fact that H₂ species adsorb weakly on the Au surface indicates that the dominant charge transfer mechanism is the indirect interfacial transfer mechanism.

On a similar note, another prominent plasmon-driven reaction is O₂ dissociation, as demonstrated for the first time by Christopher and co-workers [74]. They reported enhanced performance in the oxidation of ethylene utilizing Ag nanocubes. In the same way as H₂ dissociation, the hot electrons with sufficient energy to be transferred to LUMO, dissipate energy into the vibrational modes stretching O₂ bonds, and activating the dissociation process.

The thermodynamic basis of plasmon-assisted catalysis: In the cases above, there is a catalytic process advancing, meaning that in some way or another, there was a lowering of the transition state energy barrier; thus, lowering the activation energy (E_a). This thermodynamic basis has been experimentally evidenced in various cases [118]. Zhou et al. reported a light-induced decrease in the activation energy of ammonia decomposition under the presence of antennae-reactor Cu-Ru PNPs, from 1.21 to 0.35 kJ mol^{−1} [119]. In the case of the antioxidant hydrogen atom transfer (HAT) process achieved by hybrid

SiO₂@Ag-[Gallic-Acid], the nominal activation energy barrier was decreased by at least 1.8 kJ mol⁻¹, shown in Figure 7a,b [65]. In the case of photocatalytic Cr⁶⁺ reduction by SiO₂@Ag nanostructures, we have demonstrated a significant light-induced four-fold decrease of the activation energy (from 25.4 to 6.2 kJ mol⁻¹), depicted in Figure 7c-e [116].

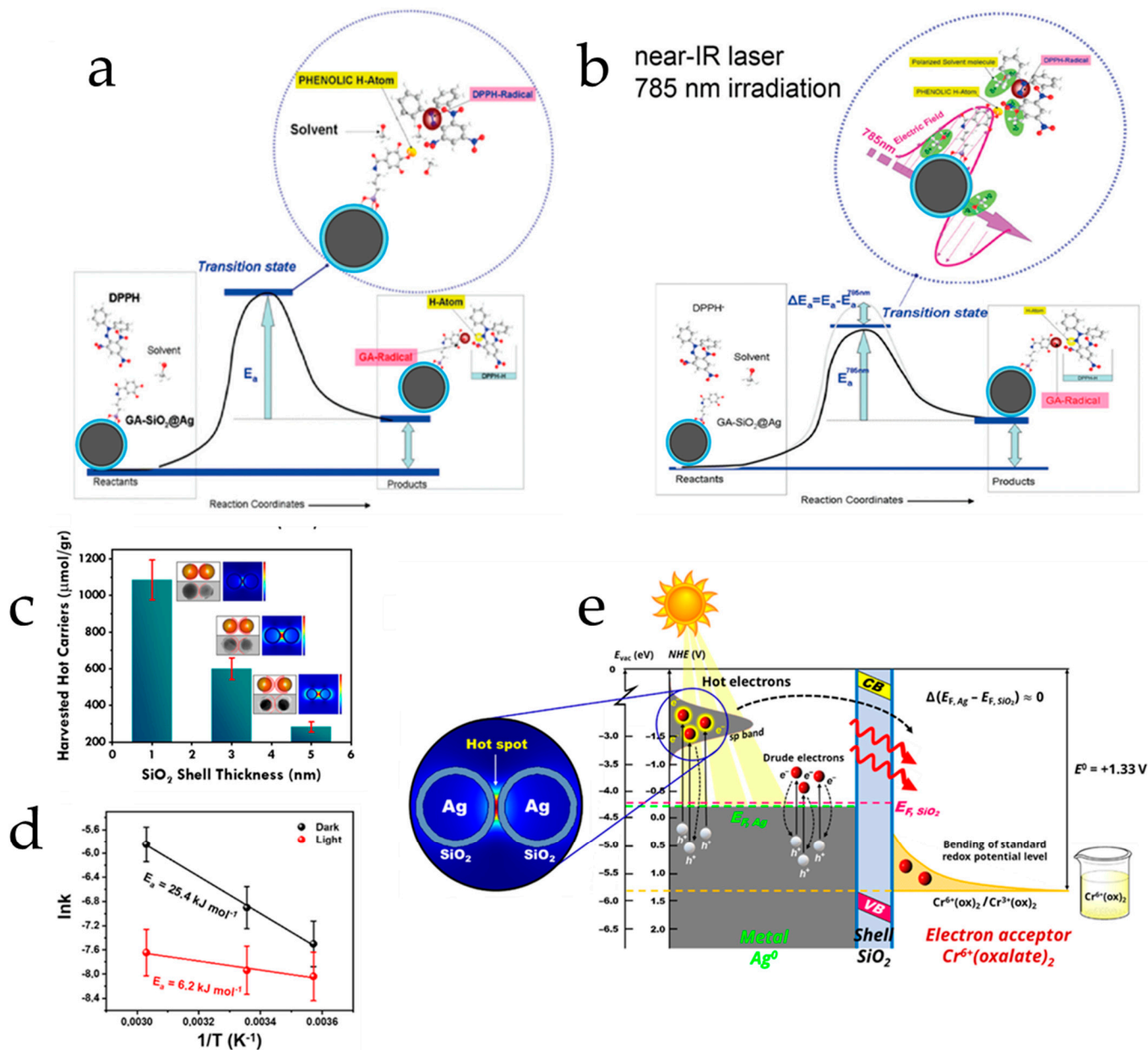


Figure 7. Reaction mechanism for the proton-coupled electron transfer from the phenolic OH of grafted GA to a DPPH radical (a) without and (b) under 785 nm laser irradiation. Adopted from the work [65]. (c) The controlled hot electron generation by illuminating core-shell Ag@SiO₂ PNPs and (d) the subsequent light-induced lowering of the activation energy. (e) The proposed mechanism of hot electron excitation and transfer to adsorbed Cr⁶⁺ species. Adapted with permission from Ref. [116], 2023, ACS.

Mechanism-wise, in the case of a hot carrier-mediated catalytic process, the plasmon-induced hot electrons, after being ejected from the metal, can decrease the activation barrier of a chemical reaction by exciting the chemically attached adsorbates, either electronically or vibrationally, unlocking the rate-limiting step for challenging chemical reactions [120,121]. Interestingly, using an illuminated plasmonic nanoparticle to change the landscape of a

chemical process can initiate reactions that would otherwise be thermodynamically and/or kinetically blocked. This opens up new possibilities for tuning the selectivity and efficiency of heterogeneous photocatalytic processes. Regarding selectivity, the metal–adsorbate interactions may enable new electron transfer channels through the hybridization of the metal’s energy levels and the adsorbate’s orbitals, so that photon energies different to LSPR and/or optical absorption of adsorbates can be harvested, triggering unique chemical pathways [122]. Here we underline that a successful plasmonic intervention to a given catalytic process that involves electron transfer requires efficient electron injection from the PNP to a proximal electron acceptor [123].

The chemical interface damping (CID) concept: Despite the promising potential of using highly energetic charge carriers to drive challenging chemical reactions, the most studied indirect charge transfer mechanism exhibits insufficient yields because of the short carrier lifetime and rapid recombination [61]. Recently, a broadening of plasmon bands in single-particle systems in contact with adsorbed/semiconducting species is attributed to a new damping process called “chemical interface damping” (CID) [124]. CID arises from the hybridization between the electronic states of the metal and the molecular orbitals of the attached species, providing a novel pathway for direct electron injection in the adsorbate [125]. The conventional indirect electron transfer is a lossy two-step mechanism, where Landau damping triggers the generation of nonthermal hot electrons with energies up to $[E_F + \hbar\omega]$, which are then injected into the LUMO of the adsorbate. However, the direct electron transfer is completed during the plasmon decay via CID, where the electron is transferred through the hybridized states. Thus, CID can be inserted into Equation (2) as an additional damping term, i.e., similar to γ_{CID} , with a similar size dependence as surface-induced damping [124,126]. This pathway is considered far more efficient and overcomes limitations such as short carrier lifetime and e–e interactions. Despite the superior electron transfer efficiency, the engineering of direct transfer is challenging since the overlap of LSPR resonance and the HOMO-LUMO transition of hybridized states is required.

On this front, Linic’s group demonstrated that degradation of methylene blue (MB) adsorbed on Ag nanocubes is induced by direct charge transfer [113]. Employing SERS, they evidenced that MB decomposition occurs under illumination at 785 nm and not 532 nm. One would expect increased efficiency from high-energy photons (532 nm) because they excite more energetic hot electrons that overcome the energy gap between Fermi level and LUMO of MB. These findings suggest that the electrons follow a CID route via Ag-MB hybridized electronic states, providing selectivity for particular chemical pathways activated exclusively by CID-induced direct electron transfer [127].

Furthermore, Seemala et al. correlated enhanced O_2 dissociation using Ag nanoparticles to CID phenomena assisted by surface electric fields [128]. The yield trend does not correspond to the calculated hot carrier density, indicating that the preferred mechanism is direct electron transfer induced by CID [128]. In both aforementioned works, the direct transfer route is ostensibly promoted by the local fields that mitigate the energy dissipation to the vibrational modes of the attached species and alleviate the dissociation process. Moreover, Christopher and co-workers demonstrated that hybridized metal adsorbate electronic states between CO and Pt surface can selectively control CO oxidation via direct electron transfer to CO-Pt bonds [129]. Thus, CID is an auspicious plasmon-induced pathway for highly efficient electron transfer that drives chemical activity in the PNP vicinity, overcoming the bottleneck of the rapidly relaxed non-thermal hot carriers. Nonetheless, the verified evidence of plasmon-driven direct transfer events in the literature remains surprisingly limited, possibly due to the complexity of the formation of resonant hybridized states and the strong chemisorption on the chemically inert surfaces of plasmonic metals such as Ag and Au.

4. Plasmon-Assisted Molecular Catalysis (PAMC)

It is well established that compared to other catalytic systems, molecular catalysts display unique reaction mechanisms providing high selectivity and activity in challenging

catalytic processes [130,131], and their usage has been extensively reviewed in numerous works [132,133]. On this front, the fundamentals of plasmon-derived mechanisms analyzed herein (hot carriers, hotspots, or thermal effects), as depicted in Figure 8, are able to enhance the activity of a molecular catalyst located in the proximity where these phenomena occur. In particular, our group has presented some key studies [84,85] which show that the plasmonic hot electrons are the primary mechanism of the observed PAMC phenomena. In [84], we have shown that plasmon-generated hot electrons could reversibly stop/start the oxidative advancement of the Mn catalytic center via “pausing on demand” the oxidation catalytic process under light excitation [84], as depicted in Figure 9. The molecular catalysis studied was alkene epoxidation in the presence of a biomimetic Mn catalyst utilizing H_2O_2 . This is based on the catalytic activation of H_2O_2 by the Mn catalyst forming a $\text{LMn}^{\text{IV}} = \text{O}$ transient intermediate. It was found that under the photoinduced action of plasmonic Ag^0/SiO_2 nanoparticles, the oxidation catalytic process can be reversibly switched off. When photoexcitation of the PNPs stops, the catalytic process recommences. Utilizing three types of plasmonic core-shell Ag^0/SiO_2 nanoparticles with a varying thickness (0.1–5 nm) SiO_2 shell, it was shown that the intensity of the observed phenomenon changed. Using EPR spectroscopy, it was demonstrated that the key step related to the photoinduced pause of the catalytic process by the Ag^0/SiO_2 PNPs is the reversible inhibition of transient $\text{LMn}^{\text{IV}} = \text{O}$ intermediate formation [84]. Moreover, the SERS and redox potential data indicated that the Ag^0/SiO_2 PNPs present a moderate SERS effect on the LMn^{II} catalyst, while the solution redox potential E_h decreases considerably [84]. Our data showed that the plasmonic heating was insignificant [84]. Therefore, the reversible switch off of the catalytic process is a result of hot electron generation by the Ag^0/SiO_2 PNPs, along with near-field generation. Overall, this work revealed a novel phenomenon, where plasmonics can act as a reversible switch for a molecular catalytic process.

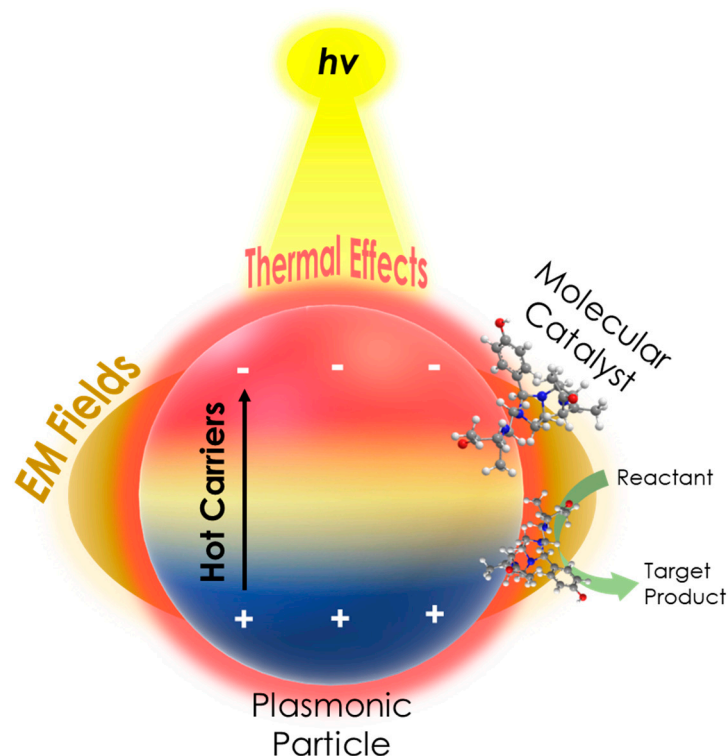


Figure 8. A schematic of the PAMC concept, illustrating the enhanced catalytic activity of a molecular catalyst in the presence of a plasmonic particle under irradiation, due to plasmonic mechanisms, i.e., hot carrier, EM fields (hotspots), and thermal effects.

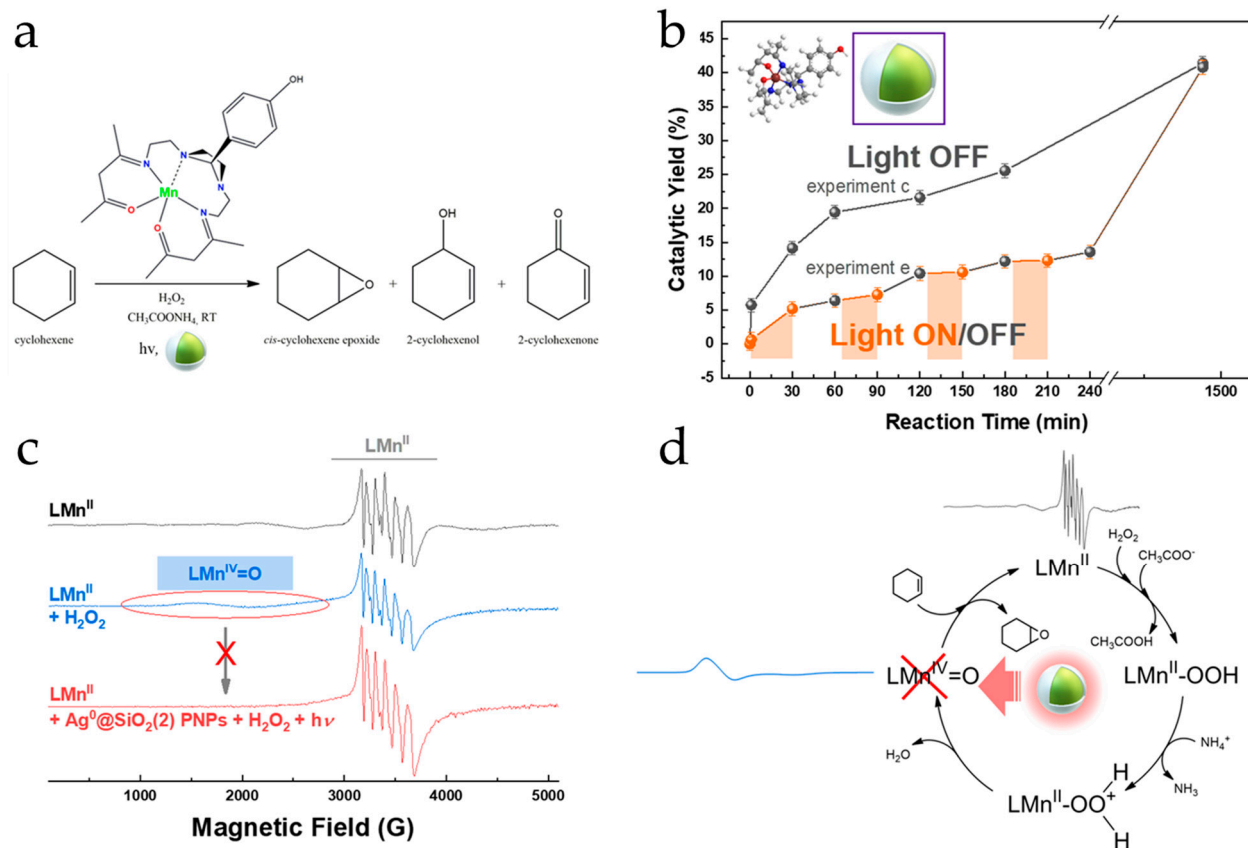


Figure 9. (a) Cyclohexene epoxidation by the [Ag⁰@SiO₂/LMn^{II}] system. (b) Reaction kinetics under no/intermittent illumination. (c) EPR spectra of the LMn^{II} catalyst and its evolution after the addition of H₂O₂ in the absence or in the presence of PNPs and illumination. (d) Established catalytic cycle of the LMn^{II} complex. Adapted with permission from Ref. [84], 2022, ACS.

In [85], we have shown that photoexcited core-shell Ag⁰@SiO₂ PNPs can dramatically enhance production of H₂ via a formic acid dehydrogenation (FADH) reaction, catalyzed by the molecular catalyst [Fe(BF₄)₂·6H₂O/P(CH₂CH₂PPh₂)₃, PP₃], see Figure 10. This is based on the catalytic activation of HCOOH by the catalyst forming a Fe-hydride transient intermediate. An almost 10-fold increase in H₂ gas production rate was achieved in the presence of photoexcited PNPs, while the TONs were boosted by ~400% and the TOFs by ~600% [85]. Through selective excitation at wavelengths (λ_{ex}) ranging over the photo-response profile of the Ag⁰@SiO₂ NPs, it was demonstrated that the enhancement on FADH is maximal at λ_{ex} = 405 nm, namely the peak of the photo-plasmonic response of the Ag⁰@SiO₂ NPs [85]. The study of the solution redox potential (E_h) under catalytic conditions showed that the excitation of the Ag⁰@SiO₂ PNPs results in hot electron injection into the reaction solution. The hot electron injection rates and the ensuing FADH rates could be controlled by varying the SiO₂-shell thickness of the Ag⁰@SiO₂ PNPs in the range of 3 nm to 5 nm. Thermoplasmonic effects, albeit not macroscopically observed, seem to play a secondary role, if any [85]. This work demonstrated the possibility to approach industrial-scale H₂ production rates via FADH, using low-cost Fe-based molecular catalysts and without any sacrificial cocatalysts.

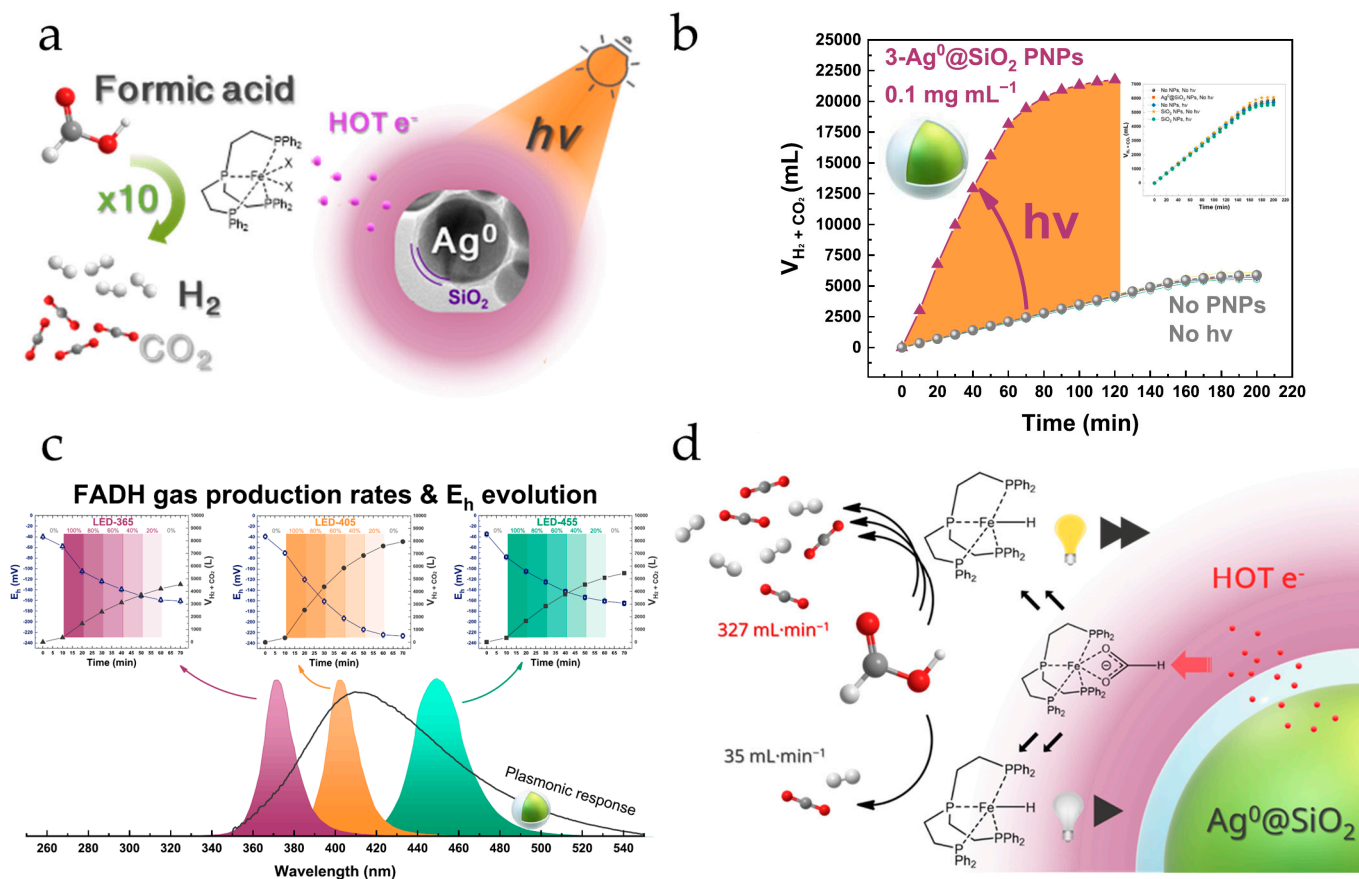


Figure 10. (a) Schematic illustration of the $[Ag^0@SiO_2/(Fe/PP_3)/HCOOH]$ catalytic system. (b) Catalytic gas production kinetics in the absence (gray circles) and presence (purple triangles) of PNPs and illumination. (c) Enhancement of H_2 production is correlated to more negative solution potentials E_h (negative ΔE_h). Both the H_2 production boosting and ΔE_h are maximized at the maximum of the plasmonic photo-response of the $Ag@SiO_2$ nanoplasmonic particles. (d) Schematic illustration of the involvement of hot electrons in the catalytic cycle of the $[Ag^0@SiO_2/(Fe/PP_3)/HCOOH]$ system. Adapted with permission from Ref. [85], 2023, ACS.

Lu et al. have found a strong synergistic relation between gold nanoparticles and cobalt porphyrin which induces highly efficient photocatalytic hydrogen evolution (Figure 11) [86]. This was another example where the catalytic activity of molecular catalysts near plasmonic nanostructures may be enhanced dramatically. The authors [86] developed a photocatalytic system for the hydrogen evolution reaction (HER) by combining a cobalt-porphyrin molecular catalyst together with plasmonic gold nanoparticles. After optimization, the HER rate and turnover frequency (TOF) reached $3.21 \text{ mol g}^{-1} \text{ h}^{-1}$ and 4650 h^{-1} , respectively. It has been demonstrated that the lifetime of plasmon-generated hot carriers is prolonged at the AuNP-CoTPyP interface, and transferred to the LUMO of CoTPyP hot carriers favoring catalytic HER. Moreover, this catalytic system could remain stable after 45 h of catalytic cycles and being illuminated for two weeks.

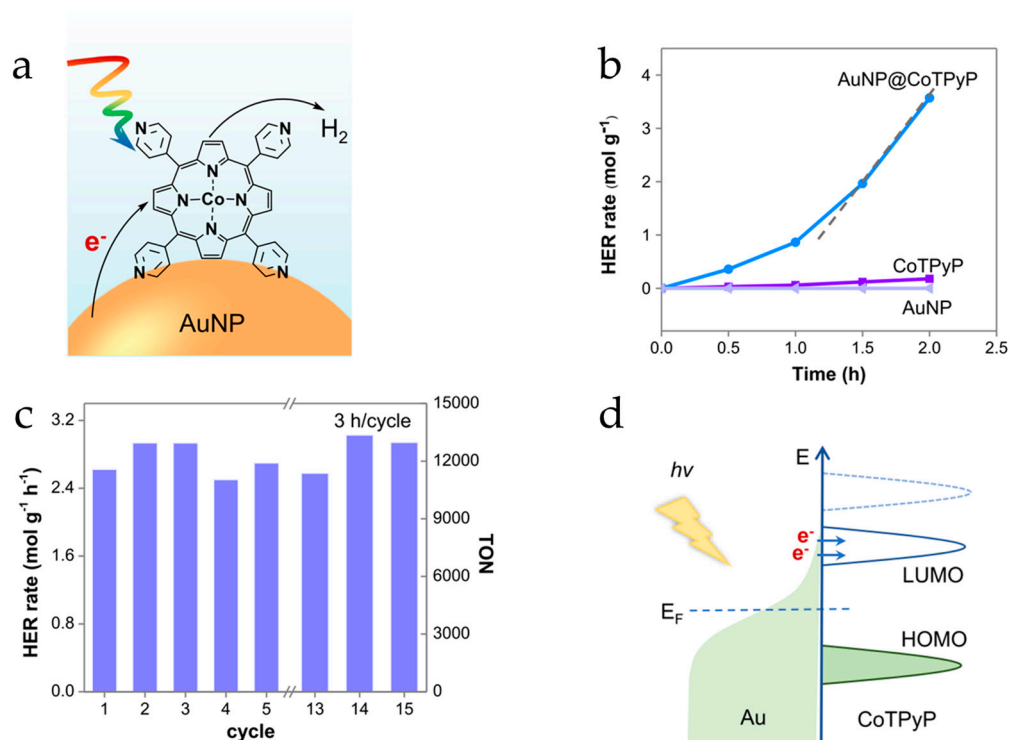


Figure 11. (a) Schematic illustration of the enhanced photocatalytic HER in AuNP@CoTPyP. (b) Photocatalytic HER curves of AuNP, CoTPyP, and AuNP@CoTPyP. (c) Photocatalytic HER cycles and the corresponding TON of AuNP@CoTPyP. (d) Schematic illustration of the charge transfer processes in AuNP@CoTPyP. Adopted from this work [86].

5. Conclusions—Future Directions

Plasmonic catalysis offers a powerful toolbox to utilize energetic electrons and heat to accelerate chemical reactions by exploitation of solar light, allowing the discovery of innovative reaction pathways. We discuss an operational classification of the fundamentals of localized surface plasmon resonance (LSPR), and of the dominant plasmon-driven mechanisms (such as hot electron generation, hotspots, plasmon decay routes, etc.). This classification allows us to comprehend the inherently complex dominant mechanisms, pertinent to the catalytic process. The concept of plasmon-promoted molecular catalysis (PAMC), i.e., the coupling of PNP to molecular catalysts, has a thermodynamic basis via activation of chemical bonds and the lowering of the activation barrier.

However, despite the bold advancements in plasmonic catalysis, moving from the “optical” hotspots (hot carriers, field enhancement, and energy transfer) to the “chemical” hotspots (reactant adsorption, CID, reaction activity, and selectivity), some critical bottlenecks need to be tackled. In particular, Cortez and co-workers [76] provided a comprehensive summary of the present challenges in the field with the most important being: [i] the creation of a theoretical model with a general description of all the possible plasmon mechanisms in photocatalysis; [ii] the complex degrees of freedom in plasmonic catalysis require the diligent control of numerous experimental parameters such as plasmonic photocatalyst characteristics (size, shape, composition, surface chemistry) and illumination settings (excitation wavelength, absorbed optical power, reactor geometry); [iii] the development and implementation of such robust plasmonic systems at relevant industrial levels; and, lastly, [iv] the design of highly efficient plasmonic devices (TRL 6–7) using abundant low-cost plasmonic materials (e.g., Al).

Author Contributions: Conceptualization, Y.D. and M.L.; methodology, C.M. and A.G.; data curation, C.M. and A.G.; writing—original draft preparation, C.M. and A.G.; writing—review and editing, Y.D. and M.L.; supervision, M.L.; project administration, Y.D. All authors have read and agreed to the published version of the manuscript.

Funding: This research received no external funding.

Data Availability Statement: No new data were created or analyzed in this study. Data sharing is not applicable to this article.

Conflicts of Interest: The authors declare no conflicts of interest.

References

1. Banerjee, A. The design, fabrication, and photocatalytic utility of nanostructured semiconductors: Focus on TiO₂-based nanostructures. *Nanotechnol. Sci. Appl.* **2011**, *4*, 35. [[CrossRef](#)] [[PubMed](#)]
2. Baffou, G.; Bordacchini, I.; Baldi, A.; Quidant, R. Simple experimental procedures to distinguish photothermal from hot-carrier processes in plasmonics. *Light. Sci. Appl.* **2020**, *9*, 108. [[CrossRef](#)] [[PubMed](#)]
3. Araujo, T.P.; Quiroz, J.; Barbosa, E.C.M.; Camargo, P.H.C. Understanding plasmonic catalysis with controlled nanomaterials based on catalytic and plasmonic metals. *Curr. Opin. Colloid Interface Sci.* **2019**, *39*, 110–122. [[CrossRef](#)]
4. Zong, C.; Xu, M.; Xu, L.-J.; Wei, T.; Ma, X.; Zheng, X.-S.; Hu, R.; Ren, B. Surface-Enhanced Raman Spectroscopy for Bioanalysis: Reliability and Challenges. *Chem. Rev.* **2018**, *118*, 4946–4980. [[CrossRef](#)] [[PubMed](#)]
5. Sheikholeslami, S.; Jun, Y.; Jain, P.K.; Alivisatos, A.P. Coupling of Optical Resonances in a Compositionally Asymmetric Plasmonic Nanoparticle Dimer. *Nano Lett.* **2010**, *10*, 2655–2660. [[CrossRef](#)]
6. Brongersma, M.L.; Halas, N.J.; Nordlander, P. Plasmon-induced hot carrier science and technology. *Nat. Nanotechnol.* **2015**, *10*, 25–34. [[CrossRef](#)]
7. Baffou, G.; Quidant, R. Nanoplasmonics for chemistry. *Chem. Soc. Rev.* **2014**, *43*, 3898–3907. [[CrossRef](#)]
8. Kim, M.; Lee, J.; Nam, J. Plasmonic Photothermal Nanoparticles for Biomedical Applications. *Adv. Sci.* **2019**, *6*, 1900471. [[CrossRef](#)]
9. Gellé, A.; Moores, A. Plasmonic nanoparticles: Photocatalysts with a bright future. *Curr. Opin. Green Sustain. Chem.* **2019**, *15*, 60–66. [[CrossRef](#)]
10. Zhao, J.; Wang, J.; Brock, A.J.; Zhu, H. Plasmonic heterogeneous catalysis for organic transformations. *J. Photochem. Photobiol. C Photochem. Rev.* **2022**, *52*, 100539. [[CrossRef](#)]
11. Zhan, C.; Chen, X.-J.; Yi, J.; Li, J.-F.; Wu, D.-Y.; Tian, Z.-Q. From plasmon-enhanced molecular spectroscopy to plasmon-mediated chemical reactions. *Nat. Rev. Chem.* **2018**, *2*, 216–230. [[CrossRef](#)]
12. Jain, V.; Kashyap, R.K.; Pillai, P.P. Plasmonic Photocatalysis: Activating Chemical Bonds through Light and Plasmon. *Adv. Opt. Mater.* **2022**, *10*, 2200463. [[CrossRef](#)]
13. Sotiriou, G.A. Biomedical applications of multifunctional plasmonic nanoparticles. *Wiley Interdiscip. Rev. Nanomed. Nanobiotechnol.* **2013**, *5*, 19–30. [[CrossRef](#)] [[PubMed](#)]
14. Brooks, J.L.; Warkentin, C.L.; Saha, D.; Keller, E.L.; Frontiera, R.R. Toward a mechanistic understanding of plasmon-mediated photocatalysis. *Nanophotonics* **2018**, *7*, 1697–1724. [[CrossRef](#)]
15. Baffou, G. *Thermoplasmonics*; Cambridge University Press: Cambridge, UK, 2017; ISBN 9781108418324.
16. Langer, J.; de Aberasturi, D.J.; Aizpurua, J.; Alvarez-Puebla, R.A.; Auguie, B.; Baumberg, J.J.; Bazan, G.C.; Bell, S.E.J.; Boisen, A.; Brolo, A.G.; et al. Present and Future of Surface-Enhanced Raman Scattering. *ACS Nano* **2020**, *14*, 28–117. [[CrossRef](#)] [[PubMed](#)]
17. Stewart, M.E.; Anderton, C.R.; Thompson, L.B.; Maria, J.; Gray, S.K.; Rogers, J.A.; Nuzzo, R.G. Nanostructured plasmonic sensors. *Chem. Rev.* **2008**, *108*, 494–521. [[CrossRef](#)] [[PubMed](#)]
18. Wadell, C.; Syrenova, S.; Langhammer, C. Plasmonic Hydrogen Sensing with Nanostructured Metal Hydrides. *ACS Nano* **2014**, *8*, 11925–11940. [[CrossRef](#)]
19. Jiang, P.; Dong, Y.; Yang, L.; Zhao, Y.; Xie, W. Hot Electron-Induced Carbon–Halogen Bond Cleavage Monitored by in Situ Surface-Enhanced Raman Spectroscopy. *J. Phys. Chem. C* **2019**, *123*, 16741–16746. [[CrossRef](#)]
20. Amendola, V.; Pilot, R.; Frascioni, M.; Maragò, O.M.; Iati, M.A. Surface plasmon resonance in gold nanoparticles: A review. *J. Phys. Condens. Matter* **2017**, *29*, 203002. [[CrossRef](#)]
21. Khurgin, J.B. Hot carriers generated by plasmons: Where are they generated and where do they go from there? *Faraday Discuss.* **2019**, *214*, 35–58. [[CrossRef](#)]
22. Camargo, P.H.C.; Cortés, E. *Plasmonic Catalysis*; Wiley: New York, NY, USA, 2021; ISBN 9783527347506.
23. Swearer, D.F.; Zhao, H.; Zhou, L.; Zhang, C.; Robotjazi, H.; Martirez, J.M.P.; Krauter, C.M.; Yazdi, S.; McClain, M.J.; Ringe, E.; et al. Heterometallic antenna-reactor complexes for photocatalysis. *Proc. Natl. Acad. Sci. USA* **2016**, *113*, 8916–8920. [[CrossRef](#)] [[PubMed](#)]
24. Joshi, G.; Mir, A.Q.; Layek, A.; Ali, A.; Aziz, S.T.; Khatua, S.; Dutta, A. Plasmon-Based Small-Molecule Activation: A New Dawn in the Field of Solar-Driven Chemical Transformation. *ACS Catal.* **2022**, *12*, 1052–1067. [[CrossRef](#)]
25. Erwin, W.R.; Zarick, H.F.; Talbert, E.M.; Bardhan, R. Light trapping in mesoporous solar cells with plasmonic nanostructures. *Energy Environ. Sci.* **2016**, *9*, 1577–1601. [[CrossRef](#)]

26. Verma, R.; Belgamwar, R.; Polshettiwar, V. Plasmonic Photocatalysis for CO₂ Conversion to Chemicals and Fuels. *ACS Mater. Lett.* **2021**, *3*, 574–598. [[CrossRef](#)]
27. Wang, D.; Pillai, S.C.; Ho, S.-H.; Zeng, J.; Li, Y.; Dionysiou, D.D. Plasmonic-based nanomaterials for environmental remediation. *Appl. Catal. B Environ.* **2018**, *237*, 721–741. [[CrossRef](#)]
28. Du, L.; Shi, G.; Zhao, Y.; Chen, X.; Sun, H.; Liu, F.; Cheng, F.; Xie, W. Plasmon-promoted electrocatalytic water splitting on metal–semiconductor nanocomposites: The interfacial charge transfer and the real catalytic sites. *Chem. Sci.* **2019**, *10*, 9605–9612. [[CrossRef](#)] [[PubMed](#)]
29. Smith, J.G.; Faucheaux, J.A.; Jain, P.K. Plasmon resonances for solar energy harvesting: A mechanistic outlook. *Nano Today* **2015**, *10*, 67–80. [[CrossRef](#)]
30. Kazuma, E.; Kim, Y. Mechanistic Studies of Plasmon Chemistry on Metal Catalysts. *Angew. Chemie Int. Ed.* **2019**, *58*, 4800–4808. [[CrossRef](#)]
31. da Silva, A.; Rodrigues, T.; Wang, J.; Camargo, P. Plasmonic catalysis with designer nanoparticles. *Chem. Commun.* **2022**, *58*, 2055–2074. [[CrossRef](#)]
32. Kreibig, U. Electronic properties of small silver particles: The optical constants and their temperature dependence. *J. Phys. F Met. Phys.* **1974**, *4*, 999–1014. [[CrossRef](#)]
33. Hartland, G.V.; Besteiro, L.V.; Johns, P.; Govorov, A.O. What’s so Hot about Electrons in Metal Nanoparticles? *ACS Energy Lett.* **2017**, *2*, 1641–1653. [[CrossRef](#)]
34. Halas, N.J.; Lal, S.; Chang, W.-S.; Link, S.; Nordlander, P. Plasmons in Strongly Coupled Metallic Nanostructures. *Chem. Rev.* **2011**, *111*, 3913–3961. [[CrossRef](#)] [[PubMed](#)]
35. Drude, P. Zur Elektronentheorie der Metalle. *Ann. Phys.* **1900**, *306*, 566–613. [[CrossRef](#)]
36. Mie, G. Beiträge zur Optik trüber Medien, speziell kolloidaler Metallösungen. *Ann. Phys.* **1908**, *330*, 377–445. [[CrossRef](#)]
37. Myroshnychenko, V.; Rodríguez-Fernández, J.; Pastoriza-Santos, I.; Funston, A.M.; Novo, C.; Mulvaney, P.; Liz-Marzán, L.M.; de Abajo, F.J.G. Modelling the optical response of gold nanoparticles. *Chem. Soc. Rev.* **2008**, *37*, 1792. [[CrossRef](#)] [[PubMed](#)]
38. Jain, P.K.; Lee, K.S.; El-Sayed, I.H.; El-Sayed, M.A. Calculated absorption and scattering properties of gold nanoparticles of different size, shape, and composition: Applications in biological imaging and biomedicine. *J. Phys. Chem. B* **2006**, *110*, 7238–7248. [[CrossRef](#)] [[PubMed](#)]
39. Bastús, N.G.; Piella, J.; Puntès, V. Quantifying the Sensitivity of Multipolar (Dipolar, Quadrupolar, and Octapolar) Surface Plasmon Resonances in Silver Nanoparticles: The Effect of Size, Composition, and Surface Coating. *Langmuir* **2016**, *32*, 290–300. [[CrossRef](#)]
40. Mulvaney, P. Surface Plasmon Spectroscopy of Nanosized Metal Particles. *Langmuir* **1996**, *12*, 788–800. [[CrossRef](#)]
41. Lincic, S.; Christopher, P.; Ingram, D.B. Plasmonic-metal nanostructures for efficient conversion of solar to chemical energy. *Nat. Mater.* **2011**, *10*, 911–921. [[CrossRef](#)]
42. Govorov, A.O.; Zhang, H.; Gun’ko, Y.K. Theory of Photoinjection of Hot Plasmonic Carriers from Metal Nanostructures into Semiconductors and Surface Molecules. *J. Phys. Chem. C* **2013**, *117*, 16616–16631. [[CrossRef](#)]
43. Govorov, A.O.; Zhang, H.; Demir, H.V.; Gun’ko, Y.K. Photogeneration of hot plasmonic electrons with metal nanocrystals: Quantum description and potential applications. *Nano Today* **2014**, *9*, 85–101. [[CrossRef](#)]
44. Stewart, S.; Wei, Q.; Sun, Y. Surface chemistry of quantum-sized metal nanoparticles under light illumination. *Chem. Sci.* **2021**, *12*, 1227–1239. [[CrossRef](#)] [[PubMed](#)]
45. Li, X.; Xiao, D.; Zhang, Z. Landau damping of quantum plasmons in metal nanostructures. *New J. Phys.* **2013**, *15*, 23011. [[CrossRef](#)]
46. Uskov, A.V.; Khurgin, J.B.; Smetanin, I.V.; Protsenko, I.E.; Nikonorov, N. V Landau Damping in Hybrid Plasmonics. *J. Phys. Chem. Lett.* **2022**, *13*, 997–1001. [[CrossRef](#)] [[PubMed](#)]
47. Sundararaman, R.; Narang, P.; Jermyn, A.S.; Goddard, W.A., III; Atwater, H.A. Theoretical predictions for hot-carrier generation from surface plasmon decay. *Nat. Commun.* **2014**, *5*, 5788. [[CrossRef](#)] [[PubMed](#)]
48. Manjavacas, A.; Liu, J.G.; Kulkarni, V.; Nordlander, P. Plasmon-Induced Hot Carriers in Metallic Nanoparticles. *ACS Nano* **2014**, *8*, 7630–7638. [[CrossRef](#)] [[PubMed](#)]
49. Dal Forno, S.; Ranno, L.; Lischner, J. Material, Size, and Environment Dependence of Plasmon-Induced Hot Carriers in Metallic Nanoparticles. *J. Phys. Chem. C* **2018**, *122*, 8517–8527. [[CrossRef](#)]
50. Besteiro, L.V.; Yu, P.; Wang, Z.; Holleitner, A.W.; Hartland, G.V.; Wiederrecht, G.P.; Govorov, A.O. The fast and the furious: Ultrafast hot electrons in plasmonic metastructures. Size and structure matter. *Nano Today* **2019**, *27*, 120–145. [[CrossRef](#)]
51. Besteiro, L.V.; Govorov, A.O. Amplified Generation of Hot Electrons and Quantum Surface Effects in Nanoparticle Dimers with Plasmonic Hot Spots. *J. Phys. Chem. C* **2016**, *120*, 19329–19339. [[CrossRef](#)]
52. Santiago, E.Y.; Besteiro, L.V.; Kong, X.-T.; Correa-Duarte, M.A.; Wang, Z.; Govorov, A.O. Efficiency of Hot-Electron Generation in Plasmonic Nanocrystals with Complex Shapes: Surface-Induced Scattering, Hot Spots, and Interband Transitions. *ACS Photonics* **2020**, *7*, 2807–2824. [[CrossRef](#)]
53. Maurice, M.S.; Barros, N.; Kachkachi, H. Orientational Selectivity of Hot Electrons Generated by a Dimer of Plasmonic Nanoparticles. *J. Phys. Chem. C* **2021**, *125*, 23991–24000. [[CrossRef](#)]
54. Besteiro, L.V.; Kong, X.-T.; Wang, Z.; Hartland, G.; Govorov, A.O. Understanding Hot-Electron Generation and Plasmon Relaxation in Metal Nanocrystals: Quantum and Classical Mechanisms. *ACS Photonics* **2017**, *4*, 2759–2781. [[CrossRef](#)]

55. Hartland, G. V Optical Studies of Dynamics in Noble Metal Nanostructures. *Chem. Rev.* **2011**, *111*, 3858–3887. [[CrossRef](#)] [[PubMed](#)]
56. Saavedra, J.R.M.; Asenjo-García, A.; García de Abajo, F.J. Hot-Electron Dynamics and Thermalization in Small Metallic Nanoparticles. *ACS Photonics* **2016**, *3*, 1637–1646. [[CrossRef](#)]
57. Narang, P.; Sundararaman, R.; Atwater, H.A. Plasmonic hot carrier dynamics in solid-state and chemical systems for energy conversion. *Nanophotonics* **2016**, *5*, 96–111. [[CrossRef](#)]
58. Huang, W.; Qian, W.; El-Sayed, M.A.; Ding, Y.; Wang, Z.L. Effect of the Lattice Crystallinity on the Electron–Phonon Relaxation Rates in Gold Nanoparticles. *J. Phys. Chem. C* **2007**, *111*, 10751–10757. [[CrossRef](#)]
59. Link, S.; El-Sayed, M.A. Spectral Properties and Relaxation Dynamics of Surface Plasmon Electronic Oscillations in Gold and Silver Nanodots and Nanorods. *J. Phys. Chem. B* **1999**, *103*, 8410–8426. [[CrossRef](#)]
60. Baffou, G.; Quidant, R. Thermo-plasmonics: Using metallic nanostructures as nano-sources of heat. *Laser Photonics Rev.* **2013**, *7*, 171–187. [[CrossRef](#)]
61. Chang, L.; Besteiro, L.V.; Sun, J.; Santiago, E.Y.; Gray, S.K.; Wang, Z.; Govorov, A.O. Electronic Structure of the Plasmons in Metal Nanocrystals: Fundamental Limitations for the Energy Efficiency of Hot Electron Generation. *ACS Energy Lett.* **2019**, *4*, 2552–2568. [[CrossRef](#)]
62. Zhang, H.; Govorov, A.O. Optical Generation of Hot Plasmonic Carriers in Metal Nanocrystals: The Effects of Shape and Field Enhancement. *J. Phys. Chem. C* **2014**, *118*, 7606–7614. [[CrossRef](#)]
63. Harutyunyan, H.; Martinson, A.B.F.; Rosenmann, D.; Khorashad, L.K.; Besteiro, L.V.; Govorov, A.O.; Wiederrecht, G.P. Anomalous ultrafast dynamics of hot plasmonic electrons in nanostructures with hot spots. *Nat. Nanotechnol.* **2015**, *10*, 770–774. [[CrossRef](#)] [[PubMed](#)]
64. Kong, X.-T.; Wang, Z.; Govorov, A.O. Plasmonic Nanostars with Hot Spots for Efficient Generation of Hot Electrons under Solar Illumination. *Adv. Opt. Mater.* **2017**, *5*. [[CrossRef](#)]
65. Sotiriou, G.A.; Blattmann, C.O.; Deligiannakis, Y. Nanoantioxidant-driven plasmon enhanced proton-coupled electron transfer. *Nanoscale* **2016**, *8*, 796–803. [[CrossRef](#)] [[PubMed](#)]
66. Marimuthu, A.; Zhang, J.; Linic, S. Tuning selectivity in propylene epoxidation by plasmon mediated photo-switching of Cu oxidation state. *Science* **2013**, *340*, 1590–1593. [[CrossRef](#)] [[PubMed](#)]
67. Lee, J.; Mubeen, S.; Ji, X.; Stucky, G.D.; Moskovits, M. Plasmonic Photoanodes for Solar Water Splitting with Visible Light. *Nano Lett.* **2012**, *12*, 5014–5019. [[CrossRef](#)] [[PubMed](#)]
68. Kim, N.H.; Meinhart, C.D.; Moskovits, M. Plasmon-Mediated Reduction of Aqueous Platinum Ions: The Competing Roles of Field Enhancement and Hot Charge Carriers. *J. Phys. Chem. C* **2016**, *120*, 6750–6755. [[CrossRef](#)]
69. Yu, Y.; Sundaresan, V.; Willets, K.A. Hot Carriers versus Thermal Effects: Resolving the Enhancement Mechanisms for Plasmon-Mediated Photoelectrochemical Reactions. *J. Phys. Chem. C* **2018**, *122*, 5040–5048. [[CrossRef](#)]
70. Sarina, S.; Zhu, H.; Jaatinen, E.; Xiao, Q.; Liu, H.; Jia, J.; Chen, C.; Zhao, J. Enhancing catalytic performance of palladium in gold and palladium alloy nanoparticles for organic synthesis reactions through visible light irradiation at ambient temperatures. *J. Am. Chem. Soc.* **2013**, *135*, 5793–5801. [[CrossRef](#)]
71. Mubeen, S.; Lee, J.; Singh, N.; Krämer, S.; Stucky, G.D.; Moskovits, M. An autonomous photosynthetic device in which all charge carriers derive from surface plasmons. *Nat. Nanotechnol.* **2013**, *8*, 247–251. [[CrossRef](#)]
72. Wang, J.; Heo, J.; Chen, C.; Wilson, A.J.; Jain, P.K. Ammonia Oxidation Enhanced by Photopotential Generated by Plasmonic Excitation of a Bimetallic Electrocatalyst. *Angew. Chem. Int. Ed.* **2020**, *59*, 18430–18434. [[CrossRef](#)]
73. Peng, H.-Y.; Xiao, Y.-H.; Yu, H.-H.; Wang, J.-Z.; Lin, J.-D.; Devasenathipathy, R.; Liu, J.; Zou, P.-H.; Zhang, M.; Zhou, J.-Z.; et al. Electrochemical and Plasmonic Photochemical Oxidation Processes of para—Aminothiophenol on a Nanostructured Gold Electrode. *J. Phys. Chem. C* **2021**, *125*, 24849–24858. [[CrossRef](#)]
74. Christopher, P.; Xin, H.; Linic, S. Visible-light-enhanced catalytic oxidation reactions on plasmonic silver nanostructures. *Nat. Chem.* **2011**, *3*, 467–472. [[CrossRef](#)] [[PubMed](#)]
75. Quiroz, J.; Barbosa, E.C.M.; Araujo, T.P.; Fiorio, J.L.; Wang, Y.-C.; Zou, Y.-C.; Mou, T.; Alves, T.V.; de Oliveira, D.C.; Wang, B.; et al. Controlling Reaction Selectivity over Hybrid Plasmonic Nanocatalysts. *Nano Lett.* **2018**, *18*, 7289–7297. [[CrossRef](#)] [[PubMed](#)]
76. Cortés, E.; Besteiro, L.V.; Alabastri, A.; Baldi, A.; Tagliabue, G.; Demetriadou, A.; Narang, P. Challenges in Plasmonic Catalysis. *ACS Nano* **2020**, *14*, 16202–16219. [[CrossRef](#)] [[PubMed](#)]
77. Wang, J.; Ando, R.A.; Camargo, P.H.C. Controlling the Selectivity of the Surface Plasmon Resonance Mediated Oxidation of *p*-Aminothiophenol on Au Nanoparticles by Charge Transfer from UV-excited TiO₂. *Angew. Chem. Int. Ed.* **2015**, *54*, 6909–6912. [[CrossRef](#)] [[PubMed](#)]
78. Zhang, X.; Li, X.; Zhang, D.; Su, N.Q.; Yang, W.; Everitt, H.O.; Liu, J. Product selectivity in plasmonic photocatalysis for carbon dioxide hydrogenation. *Nat. Commun.* **2017**, *8*, 14542. [[CrossRef](#)] [[PubMed](#)]
79. Peiris, E.; Sarina, S.; Waclawik, E.R.; Ayoko, G.A.; Han, P.; Jia, J.; Zhu, H. Plasmonic Switching of the Reaction Pathway: Visible-Light Irradiation Varies the Reactant Concentration at the Solid–Solution Interface of a Gold–Cobalt Catalyst. *Angew. Chem. Int. Ed.* **2019**, *58*, 12032–12036. [[CrossRef](#)] [[PubMed](#)]
80. Long, R.; Mao, K.; Gong, M.; Zhou, S.; Hu, J.; Zhi, M.; You, Y.; Bai, S.; Jiang, J.; Zhang, Q.; et al. Tunable Oxygen Activation for Catalytic Organic Oxidation: Schottky Junction versus Plasmonic Effects. *Angew. Chem. Int. Ed.* **2014**, *53*, 3205–3209. [[CrossRef](#)]

81. Huang, L.; Zou, J.; Ye, J.; Zhou, Z.; Lin, Z.; Kang, X.; Jain, P.K.; Chen, S. Synergy between Plasmonic and Electrocatalytic Activation of Methanol Oxidation on Palladium–Silver Alloy Nanotubes. *Angew. Chem. Int. Ed.* **2019**, *58*, 8794–8798. [[CrossRef](#)]
82. Tsukamoto, D.; Shiraiishi, Y.; Sugano, Y.; Ichikawa, S.; Tanaka, S.; Hirai, T. Gold Nanoparticles Located at the Interface of Anatase/Rutile TiO₂ Particles as Active Plasmonic Photocatalysts for Aerobic Oxidation. *J. Am. Chem. Soc.* **2012**, *134*, 6309–6315. [[CrossRef](#)]
83. Christopher, P.; Xin, H.; Marimuthu, A.; Linic, S. Singular characteristics and unique chemical bond activation mechanisms of photocatalytic reactions on plasmonic nanostructures. *Nat. Mater.* **2012**, *11*, 1044–1050. [[CrossRef](#)] [[PubMed](#)]
84. Gemenetzi, A.; Moularas, C.; Belles, L.; Deligiannakis, Y.; Louloudi, M. Reversible Plasmonic Switch in a Molecular Oxidation Catalysis Process. *ACS Catal.* **2022**, *12*, 9908–9921. [[CrossRef](#)]
85. Gemenetzi, A.; Deligiannakis, Y.; Louloudi, M. Controlled Photoplasmonic Enhancement of H₂ Production via Formic Acid Dehydrogenation by a Molecular Fe Catalyst. *ACS Catal.* **2023**, *13*, 9905–9917. [[CrossRef](#)]
86. Sheng, H.; Wang, J.; Huang, J.; Li, Z.; Ren, G.; Zhang, L.; Yu, L.; Zhao, M.; Li, X.; Li, G.; et al. Strong synergy between gold nanoparticles and cobalt porphyrin induces highly efficient photocatalytic hydrogen evolution. *Nat. Commun.* **2023**, *14*, 1528. [[CrossRef](#)] [[PubMed](#)]
87. Kale, M.J.; Avanesian, T.; Christopher, P. Direct Photocatalysis by Plasmonic Nanostructures. *ACS Catal.* **2014**, *4*, 116–128. [[CrossRef](#)]
88. Cortés, E. Activating plasmonic chemistry. *Science* **2018**, *362*, 28–29. [[CrossRef](#)] [[PubMed](#)]
89. Zhao, H.; Zheng, X.; Feng, X.; Li, Y. CO₂ Reduction by Plasmonic Au Nanoparticle-Decorated TiO₂ Photocatalyst with an Ultrathin Al₂O₃ Interlayer. *J. Phys. Chem. C* **2018**, *122*, 18949–18956. [[CrossRef](#)]
90. Robotjazi, H.; Bao, J.L.; Zhang, M.; Zhou, L.; Christopher, P.; Carter, E.A.; Nordlander, P.; Halas, N.J. Plasmon-driven carbon–fluorine (C(sp³)-F) bond activation with mechanistic insights into hot-carrier-mediated pathways. *Nat. Catal.* **2020**, *3*, 564–573. [[CrossRef](#)]
91. Pensa, E.; Gargiulo, J.; Lauri, A.; Schlücker, S.; Cortés, E.; Maier, S.A. Spectral Screening of the Energy of Hot Holes over a Particle Plasmon Resonance. *Nano Lett.* **2019**, *19*, 1867–1874. [[CrossRef](#)]
92. Zhang, Q.; Chen, K.; Wang, H. Hot-Hole-Induced Molecular Scissoring: A Case Study of Plasmon-Driven Decarboxylation of Aromatic Carboxylates. *J. Phys. Chem. C* **2021**, *125*, 20958–20971. [[CrossRef](#)]
93. Zhan, C.; Wang, Z.-Y.; Zhang, X.-G.; Chen, X.-J.; Huang, Y.-F.; Hu, S.; Li, J.-F.; Wu, D.-Y.; Moskovits, M.; Tian, Z.-Q. Interfacial Construction of Plasmonic Nanostructures for the Utilization of the Plasmon-Excited Electrons and Holes. *J. Am. Chem. Soc.* **2019**, *141*, 8053–8057. [[CrossRef](#)] [[PubMed](#)]
94. Peng, T.; Miao, J.; Gao, Z.; Zhang, L.; Gao, Y.; Fan, C.; Li, D. Reactivating Catalytic Surface: Insights into the Role of Hot Holes in Plasmonic Catalysis. *Small* **2018**, *14*, 1703510. [[CrossRef](#)] [[PubMed](#)]
95. Schlather, A.E.; Manjavacas, A.; Lauchner, A.; Marangoni, V.S.; DeSantis, C.J.; Nordlander, P.; Halas, N.J. Hot Hole Photoelectrochemistry on Au@SiO₂@Au Nanoparticles. *J. Phys. Chem. Lett.* **2017**, *8*, 2060–2067. [[CrossRef](#)] [[PubMed](#)]
96. Kontoleta, E.; Tsoukala, A.; Askes, S.H.C.; Zoethout, E.; Oksenberg, E.; Agrawal, H.; Garnett, E.C. Using Hot Electrons and Hot Holes for Simultaneous Cocatalyst Deposition on Plasmonic Nanostructures. *ACS Appl. Mater. Interfaces* **2020**, *12*, 35986–35994. [[CrossRef](#)] [[PubMed](#)]
97. Mascaretti, L.; Dutta, A.; Kment, Š.; Shalaev, V.M.; Boltasseva, A.; Zbořil, R.; Naldoni, A. Plasmon-Enhanced Photoelectrochemical Water Splitting for Efficient Renewable Energy Storage. *Adv. Mater.* **2019**, *31*, 1805513. [[CrossRef](#)] [[PubMed](#)]
98. Yuan, L.; Lou, M.; Clark, B.D.; Lou, M.; Zhou, L.; Tian, S.; Jacobson, C.R.; Nordlander, P.; Halas, N.J. Morphology-Dependent Reactivity of a Plasmonic Photocatalyst. *ACS Nano* **2020**, *14*, 12054–12063. [[CrossRef](#)]
99. Yu, S.; Wilson, A.J.; Heo, J.; Jain, P.K. Plasmonic Control of Multi-Electron Transfer and C–C Coupling in Visible-Light-Driven CO₂ Reduction on Au Nanoparticles. *Nano Lett.* **2018**, *18*, 2189–2194. [[CrossRef](#)]
100. Chen, L.-W.; Hao, Y.-C.; Guo, Y.; Zhang, Q.; Li, J.; Gao, W.-Y.; Ren, L.; Su, X.; Hu, L.; Zhang, N.; et al. Metal–Organic Framework Membranes Encapsulating Gold Nanoparticles for Direct Plasmonic Photocatalytic Nitrogen Fixation. *J. Am. Chem. Soc.* **2021**, *143*, 5727–5736. [[CrossRef](#)]
101. Devasia, D.; Wilson, A.J.; Heo, J.; Mohan, V.; Jain, P.K. A rich catalog of C–C bonded species formed in CO₂ reduction on a plasmonic photocatalyst. *Nat. Commun.* **2021**, *12*, 2612. [[CrossRef](#)]
102. Dutta, A.; Naldoni, A.; Malara, F.; Govorov, A.O.; Shalaev, V.M.; Boltasseva, A. Gap-plasmon enhanced water splitting with ultrathin hematite films: The role of plasmonic-based light trapping and hot electrons. *Faraday Discuss.* **2019**, *214*, 283–295. [[CrossRef](#)]
103. Besteiro, L.V.; Cortés, E.; Ishii, S.; Narang, P.; Oulton, R.F. Hot electron physics and applications. *J. Appl. Phys.* **2021**, *129*, 150401. [[CrossRef](#)]
104. Wu, Y.; Yang, M.; Ueltschi, T.W.; Mosquera, M.A.; Chen, Z.; Schatz, G.C.; Van Duyne, R.P. SERS Study of the Mechanism of Plasmon-Driven Hot Electron Transfer between Gold Nanoparticles and PCBM. *J. Phys. Chem. C* **2019**, *123*, 29908–29915. [[CrossRef](#)]
105. Qi, Y.; Brasiliense, V.; Ueltschi, T.W.; Park, J.E.; Wasielewski, M.R.; Schatz, G.C.; Van Duyne, R.P. Plasmon-Driven Chemistry in Ferri-/Ferrocyanide Gold Nanoparticle Oligomers: A SERS Study. *J. Am. Chem. Soc.* **2020**, *142*, 13120–13129. [[CrossRef](#)] [[PubMed](#)]
106. Takeyasu, N.; Yamaguchi, K.; Kagawa, R.; Kaneta, T.; Benz, F.; Fujii, M.; Baumberg, J.J. Blocking Hot Electron Emission by SiO₂ Coating Plasmonic Nanostructures. *J. Phys. Chem. C* **2017**, *121*, 18795–18799. [[CrossRef](#)]

107. Warren, S.C.; Thimsen, E. Plasmonic solar water splitting. *Energy Environ. Sci.* **2012**, *5*, 5133–5146. [[CrossRef](#)]
108. Zhou, L.; Martinez, J.M.P.; Finzel, J.; Zhang, C.; Swearer, D.F.; Tian, S.; Robotjazi, H.; Lou, M.; Dong, L.; Henderson, L.; et al. Light-driven methane dry reforming with single atomic site antenna-reactor plasmonic photocatalysts. *Nat. Energy* **2020**, *5*, 61–70. [[CrossRef](#)]
109. Meng, X.; Liu, L.; Ouyang, S.; Xu, H.; Wang, D.; Zhao, N.; Ye, J. Nanometals for Solar-to-Chemical Energy Conversion: From Semiconductor-Based Photocatalysis to Plasmon-Mediated Photocatalysis and Photo-Thermocatalysis. *Adv. Mater.* **2016**, *28*, 6781–6803. [[CrossRef](#)]
110. Mukherjee, S.; Libisch, F.; Large, N.; Neumann, O.; Brown, L.V.; Cheng, J.; Lassiter, J.B.; Carter, E.A.; Nordlander, P.; Halas, N.J. Hot Electrons Do the Impossible: Plasmon-Induced Dissociation of H₂ on Au. *Nano Lett.* **2013**, *13*, 240–247. [[CrossRef](#)]
111. Mukherjee, S.; Zhou, L.; Goodman, A.M.; Large, N.; Ayala-Orozco, C.; Zhang, Y.; Nordlander, P.; Halas, N.J. Hot-Electron-Induced Dissociation of H₂ on Gold Nanoparticles Supported on SiO₂. *J. Am. Chem. Soc.* **2014**, *136*, 64–67. [[CrossRef](#)]
112. Zhou, L.; Zhang, C.; McClain, M.J.; Manjavacas, A.; Krauter, C.M.; Tian, S.; Berg, F.; Everitt, H.O.; Carter, E.A.; Nordlander, P.; et al. Aluminum Nanocrystals as a Plasmonic Photocatalyst for Hydrogen Dissociation. *Nano Lett.* **2016**, *16*, 1478–1484. [[CrossRef](#)]
113. Boerigter, C.; Campana, R.; Morabito, M.; Linic, S. Evidence and implications of direct charge excitation as the dominant mechanism in plasmon-mediated photocatalysis. *Nat. Commun.* **2016**, *7*, 10545. [[CrossRef](#)] [[PubMed](#)]
114. Herran, M.; Sousa-Castillo, A.; Fan, C.; Lee, S.; Xie, W.; Döblinger, M.; Auguie, B.; Cortés, E. Tailoring Plasmonic Bimetallic Nanocatalysts toward Sunlight-Driven H₂ Production. *Adv. Funct. Mater.* **2022**, *32*, 2203418. [[CrossRef](#)]
115. Kim, Y.; Smith, J.G.; Jain, P.K. Harvesting multiple electron-hole pairs generated through plasmonic excitation of Au nanoparticles. *Nat. Chem.* **2018**, *10*, 763–769. [[CrossRef](#)] [[PubMed](#)]
116. Moularas, C.; Dimitriou, C.; Georgiou, Y.; Evangelakis, G.; Boukos, N.; Deligiannakis, Y. Electron Paramagnetic Resonance Quantifies Hot-Electron Transfer from Plasmonic Ag@SiO₂ to Cr⁶⁺/Cr⁵⁺/Cr³⁺. *J. Phys. Chem. C* **2023**, *127*, 2045–2057. [[CrossRef](#)]
117. Román Castellanos, L.; Hess, O.; Lischner, J. Dielectric Engineering of Hot-Carrier Generation by Quantized Plasmons in Embedded Silver Nanoparticles. *J. Phys. Chem. C* **2021**, *125*, 3081–3087. [[CrossRef](#)] [[PubMed](#)]
118. Kim, Y.; Dumett Torres, D.; Jain, P.K. Activation Energies of Plasmonic Catalysts. *Nano Lett.* **2016**, *16*, 3399–3407. [[CrossRef](#)]
119. Zhou, L.; Swearer, D.F.; Zhang, C.; Robotjazi, H.; Zhao, H.; Henderson, L.; Dong, L.; Christopher, P.; Carter, E.A.; Nordlander, P.; et al. Quantifying hot carrier and thermal contributions in plasmonic photocatalysis. *Science* **2018**, *362*, 69–72. [[CrossRef](#)]
120. Naldoni, A.; Riboni, F.; Guler, U.; Boltasseva, A.; Shalae, V.M.; Kildishev, A.V. Solar-Powered Plasmon-Enhanced Heterogeneous Catalysis. *Nanophotonics* **2016**, *5*, 112–133. [[CrossRef](#)]
121. Ueno, K.; Misawa, H. Surface plasmon-enhanced photochemical reactions. *J. Photochem. Photobiol. C Photochem. Rev.* **2013**, *15*, 31–52. [[CrossRef](#)]
122. Cortés, E. Efficiency and Bond Selectivity in Plasmon-Induced Photochemistry. *Adv. Opt. Mater.* **2017**, *5*, 1700191. [[CrossRef](#)]
123. Khurgin, J.B. Fundamental limits of hot carrier injection from metal in nanoplasmonics. *Nanophotonics* **2020**, *9*, 453–471. [[CrossRef](#)]
124. Lee, S.A.; Link, S. Chemical Interface Damping of Surface Plasmon Resonances. *Acc. Chem. Res.* **2021**, *54*, 1950–1960. [[CrossRef](#)] [[PubMed](#)]
125. Foerster, B.; Joplin, A.; Kaefer, K.; Celiksoy, S.; Link, S.; Sönnichsen, C. Chemical Interface Damping Depends on Electrons Reaching the Surface. *ACS Nano* **2017**, *11*, 2886–2893. [[CrossRef](#)]
126. Foerster, B.; Spata, V.A.; Carter, E.A.; Sönnichsen, C.; Link, S. Plasmon damping depends on the chemical nature of the nanoparticle interface. *Sci. Adv.* **2019**, *5*, aav0704. [[CrossRef](#)] [[PubMed](#)]
127. Boerigter, C.; Aslam, U.; Linic, S. Mechanism of Charge Transfer from Plasmonic Nanostructures to Chemically Attached Materials. *ACS Nano* **2016**, *10*, 6108–6115. [[CrossRef](#)] [[PubMed](#)]
128. Seemala, B.; Therrien, A.J.; Lou, M.; Li, K.; Finzel, J.P.; Qi, J.; Nordlander, P.; Christopher, P. Plasmon-Mediated Catalytic O₂ Dissociation on Ag Nanostructures: Hot Electrons or Near Fields? *ACS Energy Lett.* **2019**, *4*, 1803–1809. [[CrossRef](#)]
129. Kale, M.J.; Avanesian, T.; Xin, H.; Yan, J.; Christopher, P. Controlling Catalytic Selectivity on Metal Nanoparticles by Direct Photoexcitation of Adsorbate–Metal Bonds. *Nano Lett.* **2014**, *14*, 5405–5412. [[CrossRef](#)]
130. Rao, H.; Schmidt, L.C.; Bonin, J.; Robert, M. Visible-light-driven methane formation from CO₂ with a molecular iron catalyst. *Nature* **2017**, *548*, 74–77. [[CrossRef](#)]
131. Ren, S.; Joulié, D.; Salvatore, D.; Torbensen, K.; Wang, M.; Robert, M.; Berlinguette, C.P. Molecular electrocatalysts can mediate fast, selective CO₂ reduction in a flow cell. *Science* **2019**, *365*, 367–369. [[CrossRef](#)]
132. Sordakis, K.; Tang, C.; Vogt, L.K.; Junge, H.; Dyson, P.J.; Beller, M.; Laurenczy, G. Homogeneous Catalysis for Sustainable Hydrogen Storage in Formic Acid and Alcohols. *Chem. Rev.* **2018**, *118*, 372–433. [[CrossRef](#)]
133. Stathi, P.; Solakidou, M.; Louloudi, M.; Deligiannakis, Y. From Homogeneous to Heterogenized Molecular Catalysts for H₂ Production by Formic Acid Dehydrogenation: Mechanistic Aspects, Role of Additives, and Co-Catalysts. *Energies* **2020**, *13*, 733. [[CrossRef](#)]

Disclaimer/Publisher’s Note: The statements, opinions and data contained in all publications are solely those of the individual author(s) and contributor(s) and not of MDPI and/or the editor(s). MDPI and/or the editor(s) disclaim responsibility for any injury to people or property resulting from any ideas, methods, instructions or products referred to in the content.